JOURNAL OF SOLID STATE CHEMISTRY 56, 182–190 (1985)

Structural Characterization of Fe/Ti Oxide Photocatalysts by X-Ray, ESR, and Mössbauer Methods

D. CORDISCHI,* N. BURRIESCI,† F. D'ALBA,‡ M. PETRERA,§ G. POLIZZOTTI,‡ AND M. SCHIAVELLO‡

**Dipartimento di Chimica, Università "La Sapienza," Roma, †Istituto CNR Trasformazione ed Accumulo di Energia, 98013 Messina, ‡Istituto d'Ingegneria Chimica, Università di Palermo, 90128 Palermo, and §Istituto G. Donegani, Centro Ricerche Montedison, 28100 Novara, Italy*

Received March 26, 1984; in revised form July 23, 1984

The polycrystalline solids TiO_2–Fe_2O_3, with iron contents in the range 0–10 at.%, prepared by coprecipitation and by impregnation, and treated in air at temperatures in the range 500–1000°C, have been studied by X-ray, ESR, and Mössbauer methods. The TiO_2 in the samples treated at 800 and 1000°C always forms the rutile phase and the Fe^{3+} has a rather low solubility in it (~0.1 at.%). The Fe^{3+} in excess forms the antiferromagnetic pseudobrookite phase (Fe_2TiO_5). The samples treated at 500 and 650°C show a dependence on the preparation method. Those prepared by coprecipitation give at 500°C the pure anatase phase in which the Fe^{3+} has a higher solubility (≥1%); those prepared by impregnation give the anatase phase accompanied by a variable amount of rutile. The treatment at 650°C provokes the partial transformation of anatase to rutile and the complete development of the Fe_2TiO_5 phase. The relevance of these results to the photocatalytic properties shown by these solids for the photoreduction of dinitrogen to ammonia is discussed.

1. Introduction

Polycrystalline systems based on titanium oxide and transition metal oxides are of interest for the investigation of relevant aspects of solid-state chemistry and heterogeneous catalysis. In our laboratory attention has been focused on the TiO_2–Fe_2O_3 system as photocatalysts for the photoreduction of dinitrogen to ammonia in the presence of water vapor (*1–5*).

The study of this reaction has the same bearing as the water photosplitting which is currently studied in much detail by various methods and considered as the most promising candidate for photochemical solar energy conversion and storage (*6–7*). The choice of iron-ion-based materials is also of interest in the light of recent studies on the water photosplitting carried out in a photoelectrochemical device using illuminated *p*- and *n*-photoelectrodes made by Mg- and Si-doped iron oxides (*8*). In this study it has been demonstrated the feasibility of the water photosplitting reaction without any external bias.

Our photocatalytic study was carried out on powdered samples prepared by impregnation and by coprecipitation and fired at temperatures between 500 and 1000°C and with an iron content in the range 0–10 at.%.

Any attempt to interpret the photocata-

0022-4596/85 $3.00

lytic results (or any other surface process) requires, as a starting point, a detailed knowledge of the structural features of the system. Among these, the most important are the phase composition and perfection, the solubility, location, and dispersion of the Fe^{3+} ions in the different phases.

In the literature these data are rather incomplete (*9*, *10*). The present work describes the structural characterization of the catalysts by X-ray diffraction, electron spin resonance (ESR), and Mössbauer spectroscopy, and the effect of the structure on the photocatalytic properties.

2. Experimental

2.1. Materials

The catalysts were prepared by two different methods: impregnation and coprecipitation.

In the first method TiO_2 was obtained by precipitation with ammonia solution from a 15 wt% solution of $TiCl_3$ (R.P. Carlo Erba). The precipitate was carefully washed with distilled water to remove Cl^- ions and dried at 120°C. A solution of $Fe(NO_3)_3$ of known concentration was added to the precipitate, and the resulting paste was first dried at 120°C and then heated in air for 24 hr at 500, 650, 800, or 1000°C. The iron contents, as atomic percentage, were 0.05, 0.2, 0.5, 1, 2, 5, and 10.

The second series of specimens was prepared by coprecipitating iron and titanium hydroxides from the solution of $TiCl_3$ (15%) containing the desired amount of Fe^{3+} ions. The precipitates were washed with water, dried, and fired as above.

Iron-containing samples are indicated as TF, the numbers after the letters give the nominal total iron content expressed as atomic percentage and the firing temperature, respectively. Thus TF 0.2, 500 refers to a sample containing 0.2 at.% iron, fired at 500°C.

2.2. Characterization Methods.

X-Ray powder diffraction patterns were obtained at room temperature on a Philips diffractometer using Ni-filtered Cu$K\alpha$ radiation.

ESR spectra were recorded at X band on a Varian E-9 spectrometer at various temperatures. The absolute number of spins was determined on some samples from electronically integrated spectra using the Varian "strong pitch" as standard (3×10^{15} spins cm^{-1}).

Mössbauer spectra were recorded at room temperature (RT) and liquid-nitrogen temperature (77 K). Measurements were performed in the constant acceleration mode with a $^{57}Co/Rh$ source held at room temperature. Mössbauer parameters were obtained from computer fittings with Lorentzian absorption lines and least-squares optimization. The two lines of each double were constrained to have the same linewidth and intensity. The isomer shift (IS) values are always given with reference to the center of the α-Fe spectrum, which has also been used for velocity calibration.

Surface areas were determined by N_2 adsorption at 77 K on several samples, using the dynamic BET method.

3. Results and Discussion

3.1. X-Ray Analysis

The phases identified by X-ray analysis on the various samples are anatase, rutile, Fe_2TiO_5 (pseudobrookite), and α-Fe_2O_3. The catalysts are listed in Tables I and II, where the phases present, as detected by X-ray analysis, and some surface area values are reported. The thermal treatment at 500°C of samples prepared by coprecipitation yields powders which consist practically of pure anatase (Table II), whereas for the samples prepared by impregnation both anatase and rutile are generally present (Table I). The crystal size of these phases are

TABLE I

TF SAMPLES PREPARED BY IMPREGNATION: PHASES PRESENT[a] AND SOME SURFACE AREAS[b]

Sample	Firing temperature (°C)			
	500	650	800	1000
TiO_2	A++++ R+	A++ R+++	A+ R++++	R+++++
TF 0.05	A++++ R+	A+++ R++	A+ R++++	R+++++
TF 0.2	A++++ R+	A+++ R++	A(traces) R++++	R+++++
TF 0.5	A++ R+++	A+++ R++	A(traces) R++++	R+++++
Surface area	49	30	11	1
TF 1	A++++ R+	A+++ R+++	R++++ P(traces)	R+++++ P+
Surface area	47	25	8	0.8
TF 2	A++++ R+	A+++ R++ P,F(traces)	R++++ P+	R+++++ P+
Surface area	55	27		
TF 5	A+ R++++	A+ R++++ P+, F+	R+++++ P+	R+++++ P+
Surface area	32	21	6	0.4
TF 10				R+++++ P++

[a] A, anatase; R, rutile; P, pseudobrookite (Fe_2TiO_5); F, α-Fe_2O_3.
[b] Surface area: m^2g^{-1}.

very small as inferred from the broad peaks in the diffractograms.

An increase in the firing temperature favors the anatase-to-rutile transition, together with the reaction of iron and titanium oxides, and the growth of individual crystals. The diffractograms of the powders fired at 1000°C are characterized by the strong and sharp diffraction peaks of rutile, together with the much smaller but equally sharp peaks of Fe_2TiO_5 when this phase is present in detectable amounts.

A quantitative determination of the phases based on peak heights or peak areas has not been attempted, because of the dependence of these features of the diffractograms on the thermal history of each samples. Only a rough estimate of the relative abundance of the crystalline phases is therefore reported in Tables I and II, where five crosses (+++++) are given either for the predominant constituent or for the unique one present in the sample, and one cross (+) indicates a constituent present in small percentages. Crosses from two to four in number indicate intermediate percentage ranges. The term "traces" is used for phases whose peaks are barely detectable.

3.2. ESR Spectra

3.2.1. Assignment of the spectra. Three different signals due to Fe^{3+} ions in different sites were detected and assigned. These signals are called spectra I, II, and III, respectively.

Spectrum I, always present in the samples fired at 800 and 1000°C, is rather complex (Fig. 1a) being composed of six main lines at $g_1 = 8.20$, $g_2 = 5.67$, $g_3 = 3.37$, $g_4 = 2.61$, $g_5 = 1.52$, and $g_6 = 1.15$. For powders fired at 500 and 650°C this spectrum is either absent or rather weak (see below). This spectrum has been previously reported (*9, 11*) and analyzed (*11*) with the spin Hamiltonian parameters obtained from the single-crystal study of Fe^{3+} in rutile (*12*).

The shape of spectrum I does not change with recording temperature. Its intensity follows the Curie law ($I \cdot T$ = const.) quite

TABLE II

TF SAMPLES PREPARED BY COPRECIPITATION: PHASES[a] PRESENT AND SOME SURFACE AREAS[b]

Sample	Firing temperature (°C)			
	500	650	800	1000
TF 0.5	A++++	A++++ R+	R++++	R+++++
Surface area	54	30	4	0.2
TF 2	A++++ R(traces)	A++++ R+	R+++++ P+	R+++++ P+
TF 5	A+++ R(traces)	A++ R++	R++++ P+	R+++++ P+
Surface area	49	15	1	0.2
TF 10	A+++ R(traces) F(traces)	R++++ P+	R++++ P+ F(traces)	R+++++ P+ F(traces)

[a] A, anatase; R, rutile; P, pseudobrookite (Fe_2TiO_5); F, α-Fe_2O_3.
[b] Surface area: m^2g^{-1}.

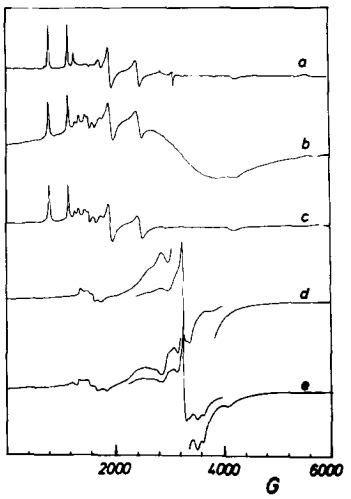

FIG. 1. ESR spectra at X band of TF samples: (a) TF 0.2, 1000°C recorded at RT; (b) TF 2, 1000°C at RT; (c) same as (b) recorded at 77 K; (d) TF 0.5, 500°C (coprecipitated) at RT; (e) same as (d) recorded at 77 K.

well, indicating that it is originated by isolated ions.

According to previous assignments, spectrum I is therefore attributed to "isolated" Fe^{3+} ions in the rutile phase.

Owing to their sharpness, the lines at g_1 and g_2 can be conveniently used for relative intensity measurements.

In the samples fired at the lowest temperatures (500 and 650°C), besides the possible presence of weak lines of spectrum I, a different spectrum is generally present (spectrum II). It consists of an intense line at $g \simeq 2.0$ having an asymmetric shape and a width of about 150 G. This line is flanked on both sides by weak shoulders (Figs. 1d and e).

Another group of lines, also belonging to the spectrum II, and having a relative intensity of $\simeq 0.04$ with respect to the main line, is present in the half-field region, i.e., at $g \simeq 4.0$.

The shape of spectrum II changes somewhat with the recording temperature, but its integrated intensity follows the Curie law quite well, which is a good indication that the spectrum II is also due to "isolated" ions.

We assign the spectrum II to "isolated" Fe^{3+} ions in the anatase phase for the following reasons. The fine terms (D and E) of Fe^{3+} in anatase, measured on a single crystal (*13, 14*), are very different from those of Fe^{3+} in rutile ($D = 0.0309$ cm^{-1}, $E = 0$ at 300°K for Fe^{3+} in anatase, and $D = 0.6788$ cm^{-1}; $E = 0.0737$ cm^{-1} for Fe^{3+} in rutile).

From these values a strong line at $g \simeq 2.0$, due to the $\frac{1}{2} \leftrightarrow -\frac{1}{2}$ transition is expected at X band for Fe^{3+} in anatase. The other allowed transitions, spread over a much larger field interval, give considerably weaker signals at their extreme values. The width of the line at $g \simeq 2.0$ is estimated to be (50/9) $(D^2/g\beta Ho) = 189$ G, in satisfactory agreement with the experimental value.

Finally, the dependence of the lineshape of spectrum II on the recording temperature is due to the unusually large variation of the D term with temperature, as found in the single crystal study (*14*).

The ESR spectra of the more concentrated samples ($[Fe^{3+}] \geq 0.5$), when recorded at room or higher temperatures, show, besides the spectrum I or spectrum II, a very large and symmetrical line ($\Delta H_{pp} \simeq 1500$ G at RT) centered at $g = 2.05$ (spectrum III) (Fig. 1b). Its linewidth changes with recording temperature and the spectrum at 77 K broadens beyond the detection limit (Fig. 1c). In contrast to the other spectra, spectrum III does not follow the Curie law, as shown in Fig. 2, where the product $I \cdot T$ (integrated intensity × temperature) is reported as a function of the recording temperature.

This behavior is typical of a paramagnetic species in a concentrated system with antiferromagnetic interactions.

The comparison with X-ray data indicates the presence of spectrum III only in samples which contain Fe_2TiO_5. We therefore assign the spectrum III to Fe^{3+} ions in the Fe_2TiO_5 phase.

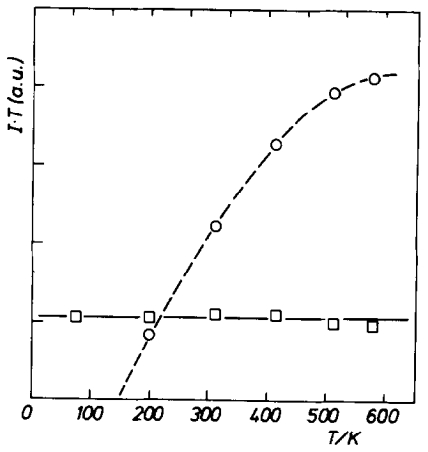

FIG. 2. Dependence of $I \cdot T$ (arbitrary units) on the recording temperature for spectrum I (□) (line g_1) and for spectrum III (integrated spectrum) (○). Sample TF 2, 1000°C.

3.2.2. Factors affecting the intensity of the ESR spectra. The occurrence and the intensity of the spectra described in the previous section depend on several factors: iron content, firing temperature, and preparation method.

The samples fired at high temperatures show a better reproducibility and therefore they will be considered first:

(i) Samples fired at 800 and 1000°C. The samples fired at these temperatures show only spectrum I, and spectrum III (for $[Fe^{3+}] \geq 0.5$).

The intensity of spectrum I for samples fired at 800 and 1000°C increase with iron content up to a limiting value, as shown in Fig. 3. The trend of the curve of Fig. 3 indicates that in the more concentrated samples only a fraction of the total iron contributes to the spectrum I.

From the integrated spectra a value of ~0.1 at.% (with a possible error of a factor of 2) has been estimated as the maximum concentration of Fe^{3+} in the rutile phase, i.e., a concentration much smaller than the nominal one for the more concentrated samples.

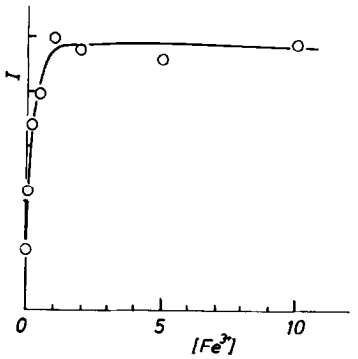

FIG. 3. Intensity (arbitrary units) of spectrum I (line g_1) for the TF samples treated at 1000°C versus the total iron content. $[Fe^{3+}] = Fe^{3+}$ atoms/100 Ti atoms.

Conversely, the intensity of spectrum III increases linearly with the iron content, and is practically independent of firing temperature (Fig. 4). Although no reliable evaluation of the number of spins can be obtained from the integrated spectra, because of the very broad linewidth and the deviation from the Curie law of spectrum III, the straight line of Fig. 4 passing across the origin, indicates that in the more concentrated samples a large fraction of the iron present contributes to the spectrum III.

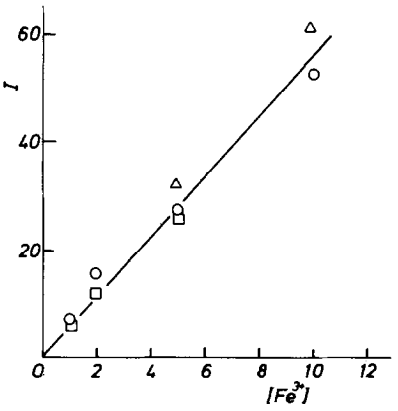

FIG. 4. Intensity (arbitrary units) of spectrum III (integrated spectra) versus the total iron content for TF samples treated at (○) 1000°C; (□) 800°C; (△) 650°C (coprecipitated).

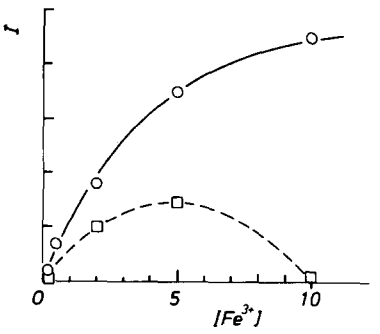

FIG. 5. Intensity (arbitrary units) of spectrum II (integrated spectra) versus the total iron content for coprecipitated samples treated at (○) 500°C; (□) 650°C.

The ESR spectra therefore confirm the X-ray findings about the presence of the phase Fe_2TiO_5 on the more concentrated samples, and allow the solubility of Fe^{3+} in the rutile phase to be measured.

(ii) Samples fired at 500 and 650°C. As stated above, the occurrence and intensity of the various spectra depend on both firing temperature and preparation method. For a given iron content, the samples prepared by coprecipitation and fired at 500°C, show the most intense spectrum II without the presence of spectrum I.

In the more concentrated samples (TF 5 and TF 10), spectrum III is also present as a weak and very broad line ($\Delta H_{pp} \simeq 2.000$ G). Its intensity is about 0.2–0.4 that of the corresponding sample fired at higher temperatures. The dependence of the intensity of spectrum II on iron content for these samples is reported in Fig. 5. The trend is similar to that of Fig. 3, but in this case the maximum value is reached at a much higher iron content and the integrated intensity is about 10 times higher than that of spectrum I. This result indicates that the solubility limit of Fe^{3+} in the anatase phase is substantially higher (~1 at.%) than in the rutile phase (~0.1 at.%).

Firing this samples at 650°C drastically reduces the intensity of spectrum II (Fig. 5), and provokes the appearance of a weak spectrum I, and, in the concentrated samples, a marked increase of the intensity of spectrum III.

The samples prepared by impregnation and fired at 500 and 600°C show, in general, both spectra I and II. The intensity of spectrum I is weak and shows a poor correlation with the iron content.

The intensity of the spectrum II follows a trend similar to that of the coprecipitated samples, but a larger variability is observed.

3.3. Mössbauer Spectra

Mössbauer spectroscopy of ^{57}Fe offers a convenient means for the phase composition analysis of TF catalysts with nominal iron content ≥2 at.%. The evolution during thermal activation can be followed through the variation of the Mössbauer parameters calculated from the experimental spectra.

As seen from Fig. 6, the spectra are always represented at 77 K by a quadrupole-

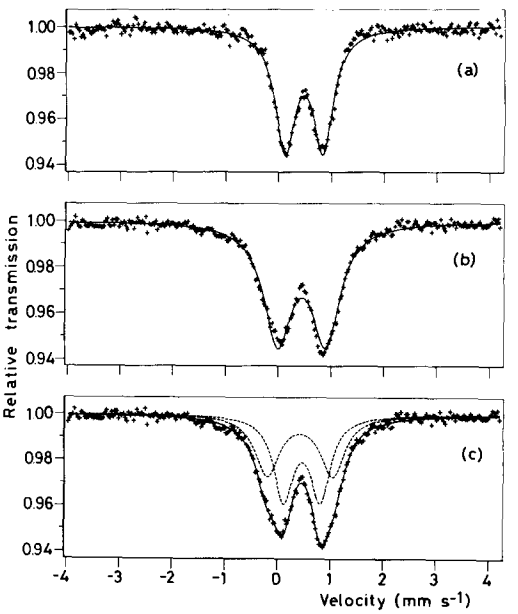

FIG. 6. Mössbauer spectra of TF samples at 80 K: (a) TF 5, 1000°C; (b) TF 10, 500°C; (c) TF 10, 500°C alternative fitting. All samples from the coprecipitated series.

TABLE III

MÖSSBAUER PARAMETERS AT 80 K OF TF CATALYSTS (mm sec^{-1})[a]

Coprecipitated samples	IS[b]	QS	Γ	χ^2
TF 2, 500	0.46(2)	0.93(2)	0.75(2)	1.04
TF 2, 1000	0.48(1)	0.78(1)	0.51(1)	1.13
TF 5, 500	0.46(1)	0.87(1)	0.63(1)	1.32
TF 5, 650	0.50(1)	0.76(1)	0.59(1)	1.12
TF 5, 800	0.50(1)	0.74(1)	0.48(1)	1.16
TF 5, 1000	0.48(1)	0.72(1)	0.46(1)	1.11
TF 10, 500	0.46(1)	0.91(1)	0.64(1)	1.80
TF 10, 650	0.48(1)	0.72(1)	0.50(1)	1.93
TF 10, 800	0.48(1)	0.73(1)	0.50(1)	1.00
TF 10, 1000	0.51(1)	0.73(1)	0.49(1)	1.05
TF 5, 500[c]	0.44(2)	1.15(2)	0.58(2)	0.87
	0.48(1)	0.64(1)	0.48(1)	
TF 10, 500[c]	0.44(2)	1.24(2)	0.56(1)	1.04
	0.48(1)	0.70(1)	0.45(1)	
Impregnated samples				
TF 5, 500	0.42(2)	0.83(2)	0.75(2)	0.92
TF 5, 1000	0.44(1)	0.72(1)	0.58(1)	1.25
Fe_2TiO_5	0.45(1)	0.73(1)	0.54(1)	

[a] Mean standard deviations are given in parenthesis.
[b] Relative to α-Fe.
[c] Alternative fitting with two doublets.

split resonance. From the data reported in Table III the observed resonance pattern is attributed to the presence of Fe_2TiO_5 (pseudobrookite) in all the samples with the exception of those fired at 500°C, which show a definitely higher value of quadrupole splitting (QS) (~0.9 mm sec^{-1} for coprecipitated TF) and broader absorption lines (see Fig. 6c). This result may be interpreted assuming that significant distortions are found in the pseudobrookite structure for relatively low firing temperatures, where crystallization and sintering of the particles is still incomplete. Another explanation is that at such temperatures a second Fe^{3+}-containing phase is still present, which is transformed into Fe_2TiO_5 with higher temperature treatment. In fact, a significant improvement in the goodness-of-fit parameter χ^2 was obtained in the case of TF 10,500°C by an alternative fitting including two doublets (Fig. 6c). This second fitting accounts for a doublet with the parameters of Fe_2TiO_5 and another one with about the same IS and a much larger QS (1.24 mm sec^{-1}), indicating the presence of a different ferric compound with relative intensity of about 47%.

Only on the basis of the Mössbauer data, the attribution of the latter component is not straightforward.

Superparamagnetic hematite particles should be excluded considering their QS value which is nearly 0.8 mm sec^{-1} (*15*).

However, as discussed in the previous section, the solubility of Fe^{3+} in anatase has been estimated by ESR to be about 1% (or possibly higher), i.e., an order of magnitude higher than in rutile phase and at a value which permits its detection by Mössbauer spectroscopy.

We therefore assign the component with QS = 1.24 mm sec^{-1} to the Fe^{3+} ions in solid solution in the anatase phase.

It is worth noting to observe that the component with QS = 0.53, which is the value reported in the literature for Fe^{3+} in rutile (*16*), has never been detected in our samples indicating that the Fe^{3+} concentration in the rutile phase remains always under the detection limit.

4. Conclusions

4.1. Main Structural Features of the TF System

After the analysis of the results of the various techniques used in the present investigation it is useful to compare them and give a synopsis of the main conclusions which can be drawn on the TF system.

(i) The features of the samples fired at 800 and 1000°C are largely independent on the preparation method. The TiO_2 always forms the rutile phase, and the Fe^{3+} has a rather low solubility in it (~0.1 at.%). The Fe^{3+} in excess forms the pseudobrookite (Fe_2TiO_5) phase, which is antiferromagnetic.

The solubility value of Fe^{3+} in rutile is in good agreement with that (0.19 at.%) found by Johnson *et al.* (*17*) on a rutile single crystal doped with $FeCl_3$ at 800°C in an atmosphere of H_2O and O_2. As these authors pointed out, the Fe^{3+} ions enter in solid solution as substitutional ions together with H^+ ions, which diffuse easily in the rutile structure (*18*). When H_2O is completely removed from the atmosphere the solubility of Fe^{3+} strongly decreases (*17*). The H^+ ions, associated with nearby O^{2-} ions, are normally located far from the Fe^{3+} ions, whereas a few of them are near Fe^{3+} ions, which therefore give a different ESR spectrum, as revealed by a single-crystal study (*19*).

(ii) The samples fired at 500 and 650°C show a dependence on the preparation method.

Those prepared by coprecipitation show the most reproducible and uniform behavior. After firing at 500°C the pure anatase phase is formed. In this phase Fe^{3+} has a much higher solubility ($\geq$1%) than in rutile. In the more concentrated samples (TF 5 and TF 10) the Fe_2TiO_5 phase is also detected, but it is less abundant and more defective than in the samples fired at higher temperatures.

In the samples prepared by impregnation, and fired at 500°C, the anatase phase is accompanied by variable amounts of the rutile phase.

The firing at 650°C provokes partial transformation of anatase to rutile at a level depending on the iron content (Fig. 5) and the development of the Fe_2TiO_5 and α-Fe_2O_3 phases.

The surface area decreases steadily with increasing temperature.

4.2. Comment on the Photocatalytic Behavior in Relation to the Structural Properties

The essential results of the photocatalytic study are reported in detail elsewhere (*1–5*). Briefly, though:

—Only specimens containing Fe^{3+} in an appropriate amount, 0.5–1.0 at.%, are active, the ammonia production being 50–100 μg/hr for 1 g of catalyst. Among these catalysts, those prepared by coprecipitation are the most active.

—The specimens in which the phase Fe_2TiO_5 is detectable by X-ray, are completely inactive.

—Pure TiO_2 (anatase and rutile) and pure Fe_2TiO_5 are also inactive.

—Ammonia was not produced in the absence of water, light, or the catalyst.

Some aspects of the photocatalytic data may be rationalized looking at the structural features of the Fe_2O_3–TiO_2 system. Essentially the catalyst phase composition affects the photocatalytic behavior; more precisely the ferric ions in solid solution in the TiO_2 lattice seem to be responsible for the origin of the photoactivity. Indeed pure oxides, TiO_2 and Fe_2TiO_5, and the catalysts containing ferric ions in the Fe_2TiO_5 phase are almost completely inactive.

This special role of Fe^{3+} can be understood considering the main steps of a photocatalytic reaction: (a) photogeneration of hole and electron pairs which must be trapped to avoid recombination; (b) reduction and oxidation reactions by the separated electrons and holes with suitable adsorbed species; (c) evolution of intermediates, desorption of products and reconstruction of the surface.

While the discussion of the reaction mechanism can be found elsewhere (*1, 2*), we suggest that the ferric ions mainly influence steps (a) and (b). Reflectance spectra (*5*) show that the ferric ions dispersed in the TiO_2 lattice (solid solution) little affect the radiation absorption properties of the TiO_2. This finding implies that the photogeneration of hole and electron pairs from TiO_2 is not (or only very marginally) affected by the presence of Fe^{3+} ions. Therefore, undoped TiO_2 being inactive, the ferric ions exhibit their role acting as electron traps, thus enhancing the charge separation. This

same role has been involved in a recent electrochemical investigation (*20*).

In addition to this we have also suggested that ferric ions play a role in the charge-transfer mechanism via a cooperative effect with the Ti^{4+}/Ti^{3+} couple, according to the mechanism

$$Ti^{3+} + Fe^{3+} \rightarrow Ti^{4+} + Fe^{2+}$$

$$Fe^{2+} \xrightarrow{h\nu} Fe^{2+,*}$$

$$Fe^{2+,*} + Ox \rightarrow Fe^{3+} + R$$

$$Ti^{3+} + Ox \xrightarrow{h\nu} Ti^{4+} + R$$

where Ox and R are oxidized and reduced adsorbed species, respectively.

In conclusion the paper reports a rather detailed characterization of the Fe/Ti oxides system which represents an example of a photocatalytic system interesting for its potential for the photochemical conversion of solar energy.

The correlations among structural results and photocatalytic features must be considered qualitative and further studies are needed for elucidating other aspects.

References

1. V. Augugliaro, A. Lauricella, L. Rizzuti, M. Schiavello, and A. Sclafani, *Int. J. Hydrogen Energy* **7,** 845 (1982).
2. V. Augugliaro, F. D'Alba, L. Rizzuti, M. Schiavello, and A. Sclafani, *Int. J. Hydrogen Energy* **7,** 851 (1982).
3. M. Schiavello, L. Rizzuti, A. Sclafani, I. Majo, V. Augugliaro, and P. L. Yue, "Proceedings, 4th World Hydrogen Energy Conference, Pasadena," p. 821 (1982).
4. A. Brucato, I. Majo, A. Sclafani, and M. Schiavello, "Proceedings, 4th International Conference Photochemical Conversion and Storage of Solar Energy, Jerusalem (Israel)," p. 116 (1982).
5. M. Schiavello, L. Rizzuti, R. I. Bickley, J. A. Navio, and P. L. Yue, "Proceedings, 8th International Congress on Catalysis, Berlin (West), 2–6 July 1984," Vol. III, p. 383, Verlag Chemie, Weinheim (1984).
6. M. Grätzel, "Photochemical Conversion and Storage of Solar Energy" (J. S. Connolly, Ed.), p. 131, Academic Press, New York (1981), and references therein.
7. J. M. Lehn, "Photochemical Conversion and Storage of Solar Energy" (J. S. Connolly, Ed.), p. 161, Academic Press, New York (1981), and references therein.
8. L. Leygraf, M. Hendewerk, and G. A. Somorjai, *J. Catal.* **78,** 341 (1982).
9. N. G. Maksimov, J. L. Mikhailova, and V. F. Anufrienko, *Kinet. Catal. (Engl. Transl.)* **13,** 1162 (1973).
10. B. J. Tatarchuk and J. A. Dumesic, *J. Catal.* **70,** 308 (1981).
11. D. Cordischi, M. Valigi, D. Gazzoli, and V. Indovina, *J. Solid State Chem.* **15,** 82 (1975).
12. D. L. Carter and A. Okaya, *Phys. Rev.* **118,** 1485 (1960).
13. D. Gainon and R. Lacroix, *Proc. Phys. Soc. (London)* **79,** 658 (1962).
14. M. Horn and C. F. Schwerdtfeger, *J. Phys. Chem. Solids* **32,** 2529 (1971).
15. T. Nakamura, T. Shinjo, Y. Endoh, N. Yamamoto, M. Shiga, and Y. Nakamura, *Phys. Lett.* **12,** 178 (1964).
16. V. K. Yarmarkin, S. P. Teslenko, and A. I. Knyazev, *Phys. Status Solidi A* **45,** 63 (1978).
17. O. W. Johnson, J. DeFord, and J. W. Shaner, *J. Appl. Phys.* **44,** 3008 (1973).
18. J. V. Cathcart, R. A. Perkins, J. B. Bates, and L. C. Manley, *J. Appl. Phys.* **50,** 4110 (1979).
19. P. D. Andersson and E. L. Kollberg, *Phys. Rev. B* **8,** 4956 (1973).
20. M. O. Ward, J. R. White, and A. J. Bard, *J. Amer. Chem. Soc.* **105,** 27 (1983).